SUPPORTING INFORMATION

Unexpected Roles of a Tether Harboring a Tyrosine Gatekeeper Residue in Modular Nitrite Reductase Catalysis

Tobias M. Hedison[1], Rajesh Shenoy[2], Andreea I. Iorgu[1], Derren J. Heyes[1], Karl Fisher[1], Gareth S. A. Wright[2], Sam Hay[1], Robert R. Eady[2], Svetlana V. Antonyuk[2], S. Samar Hasnain[2]*, Nigel S. Scrutton[1]*

[1]Manchester Institute of Biotechnology and School of Chemistry, Faculty of Science and Engineering, The University of Manchester, 131 Princess Street, Manchester M1 7DN, United Kingdom

[2]Institute of Integrative Biology, Faculty of Health and Life Sciences, University of Liverpool, Liverpool L69 7ZB, United Kingdom

*Corresponding authors:

Nigel Scrutton, email: nigel.scrutton@manchester.ac.uk, and Samar Hasnain, email: s.s.hasnain@liverpool.ac.uk

Table of Contents

Design of Deconstructed *Ralstonia Pickettii* Copper Containing Nitrite Reductase Constructs

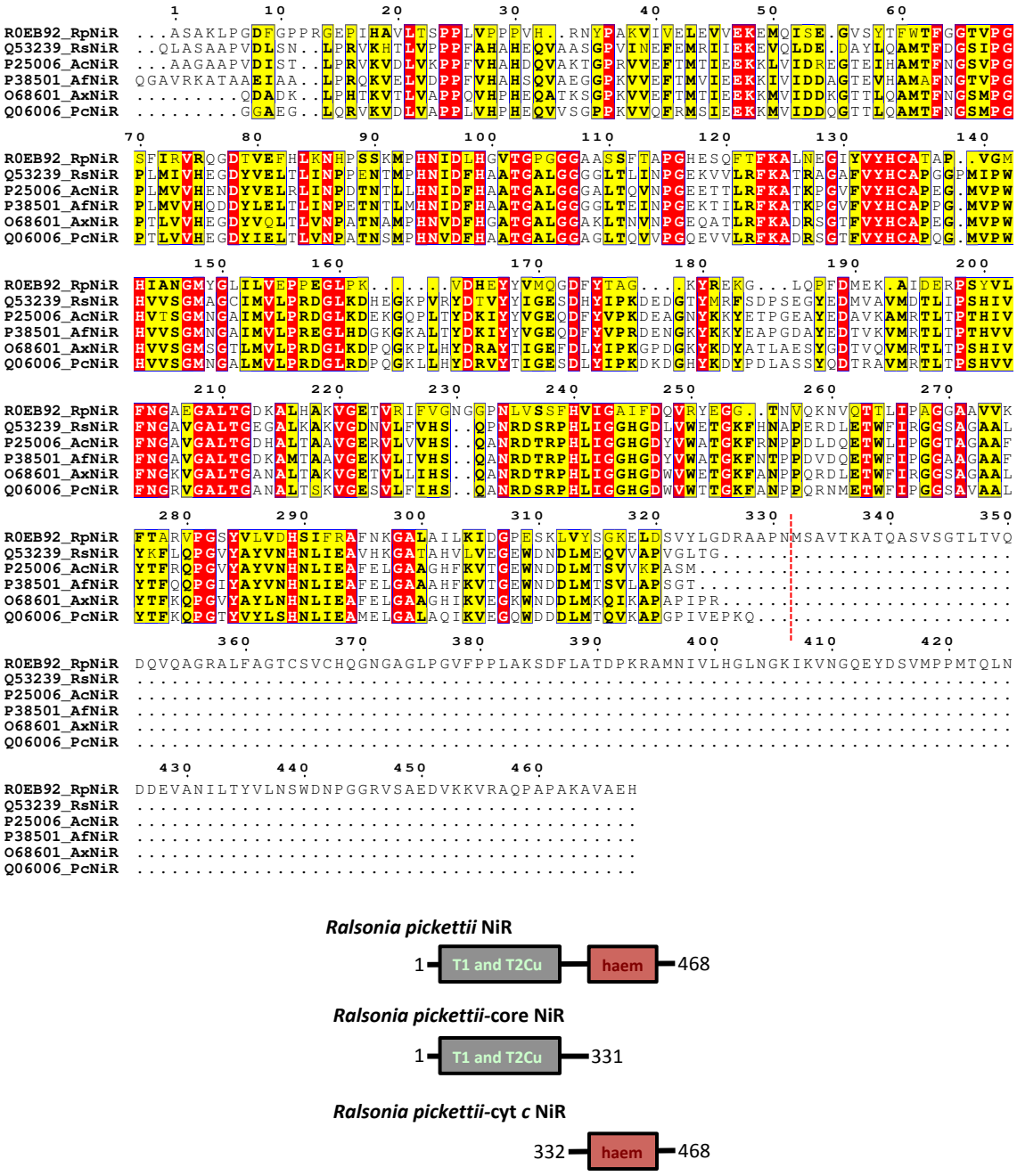

Figure S1. Multiple sequence alignment of selected 2-domain copper containing nitrite reductases with *Ralstonia pickettii* copper nitrite reductase and design of synthetic components. Top) Sequence alignment. Residues highlighted in red are conserved among all selected CuNiRs, while those highlighted in yellow are only partially conserved/sharing similar physico-chemical properties. The multiple sequence alignment was performed using the Clustal Omega web server, and the alignment file was rendered using the ENDscript server.[1] Each line on the first column of the figure is showing the Uniprot accession code followed by the shorthand name of each copper containing nitrite reductase. All N-terminal leader sequences, which are cleaved in the periplasmic space to produce the mature CuNiR proteins, have been omitted from the sequence alignment for simplicity. **Bottom)** A schematic of the full-length and deconstructed *Rp*NiR protein. The *Rp*NiR protein (top of schematic) is numbered from the N-terminus to the C-terminus and excludes the N-terminal leader sequence (residues 1-31), which is cleaved to produce the mature protein after *Rp*NiR is directed to the periplasmic space. The *Rp*NiR core protein (middle of schematic) and the *Rp*NiR cytochrome *c* protein (bottom of schematic) are numbered in relation to the mature full-length *Rp*NiR enzyme. In the schematic, the core portion is shown as a grey rectangle and the cytochrome *c* domain is shown as a red square.

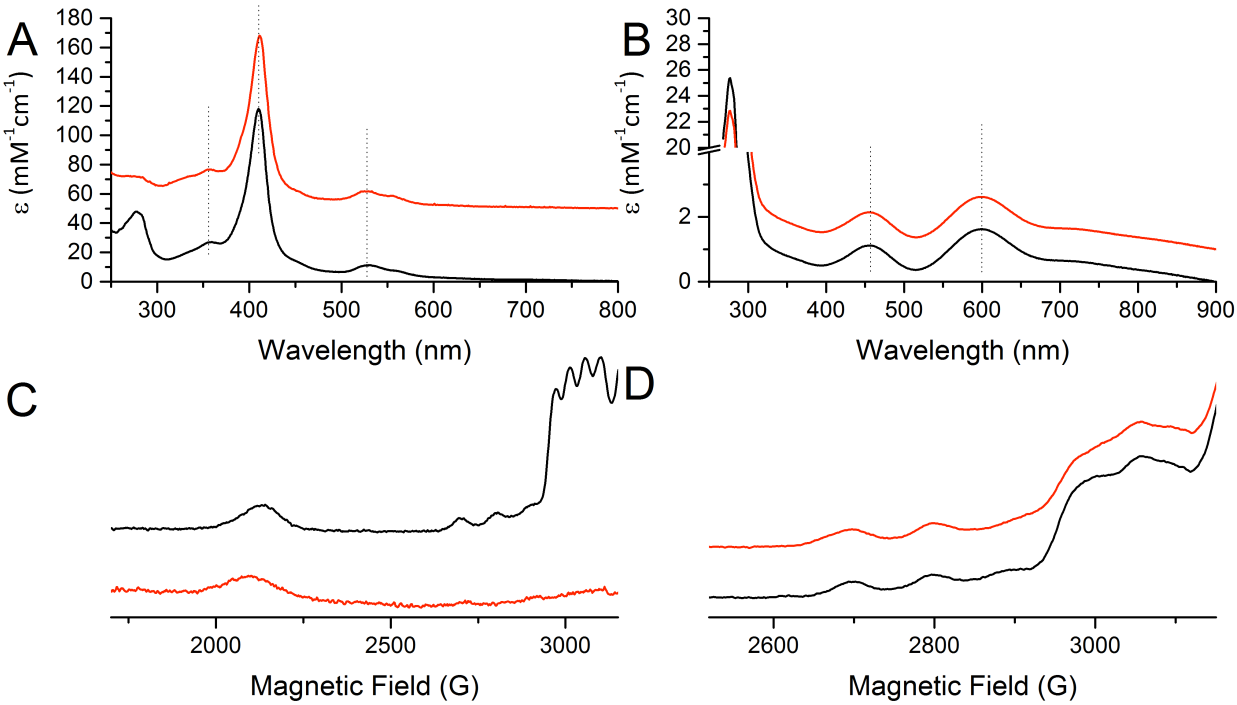

Figure S2. UV-Vis and EPR spectroscopic properties of the different *Ralstonia pickettii* CuNiR constructs used in this investigation. A) UV-Vis spectra of oxidised wild-type (black) and cytochrome *c* (red) *Rp*NiR constructs. **B)** UV-Vis spectra of the oxidised *Rp*NiR-core (black) and Y323F *Rp*NiR-core (red) constructs. In A) and B), spectra have been shifted on the *y*-axis for a clear comparison between the different *Rp*NiR constructs. In A), the *Rp*NiR cytochrome *c* spectra has been shifted by a factor of +50 $mM^{-1}cm^{-1}$, while in B), the Y323F *Rp*NiR-core has been shifted by a factor of 1 $mM^{-1}cm^{-1}$, respectively. **C)** EPR spectra of oxidised wild-type (black) and cytochrome c (red) *Rp*NiR constructs. **D)** EPR spectra of oxidised *Rp*NiR-core (black) and Y323F *Rp*NiR-core (red) constructs. All UV-Vis measurements were performed in 50 mM potassium phosphate buffer (pH 7.0), at 25 °C. All EPR measurements were performed in 50 mM potassium phosphate buffer (pH 7.0) with 80-130 uM protein samples. EPR measurements were performed at 20 K on a Bruker EMX X-band EPR spectrometer. The microwave power was 0.5 mW, the modulation frequency 100 kHz, and the modulation amplitude 5 G.

'Compactness' of the *Rp*NiR-Core Trimer

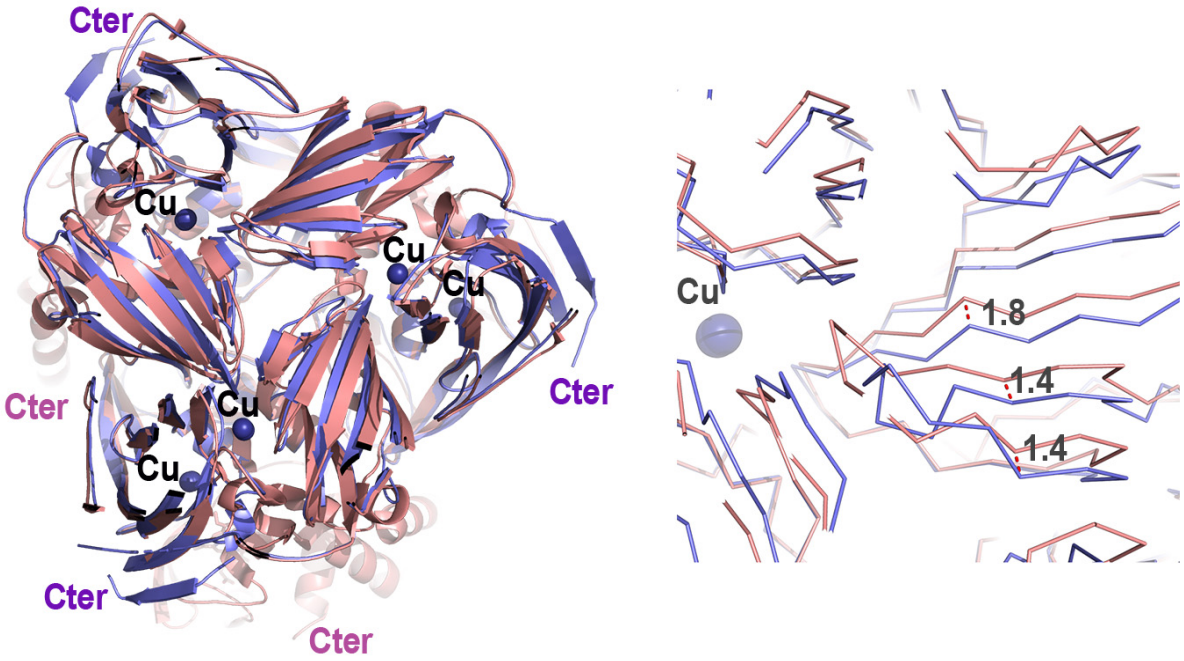

Figure S3. Structural alignment of the *Rp*NiR-core and the full-length *Rp*NiR (PDB ID: 3ZIY) trimers. Left) The displayed alignment shows an increase in compactness of the *Rp*NiR-core (lilac) when compared with the full-length *Rp*NiR trimer (salmon). **Right)** A zoomed section of the structural alignment showing the average inward movement of ~1.6 Å of the *Rp*NiR-core β-strands when compared to the full-length *Rp*NiR. Copper ions (Cu) are shown as dark blue spheres and the visible C-terminals of full-length and core *Rp*NiR proteins are denoted by C-ter.

Details of T2Cu Nitrite Bound Sites

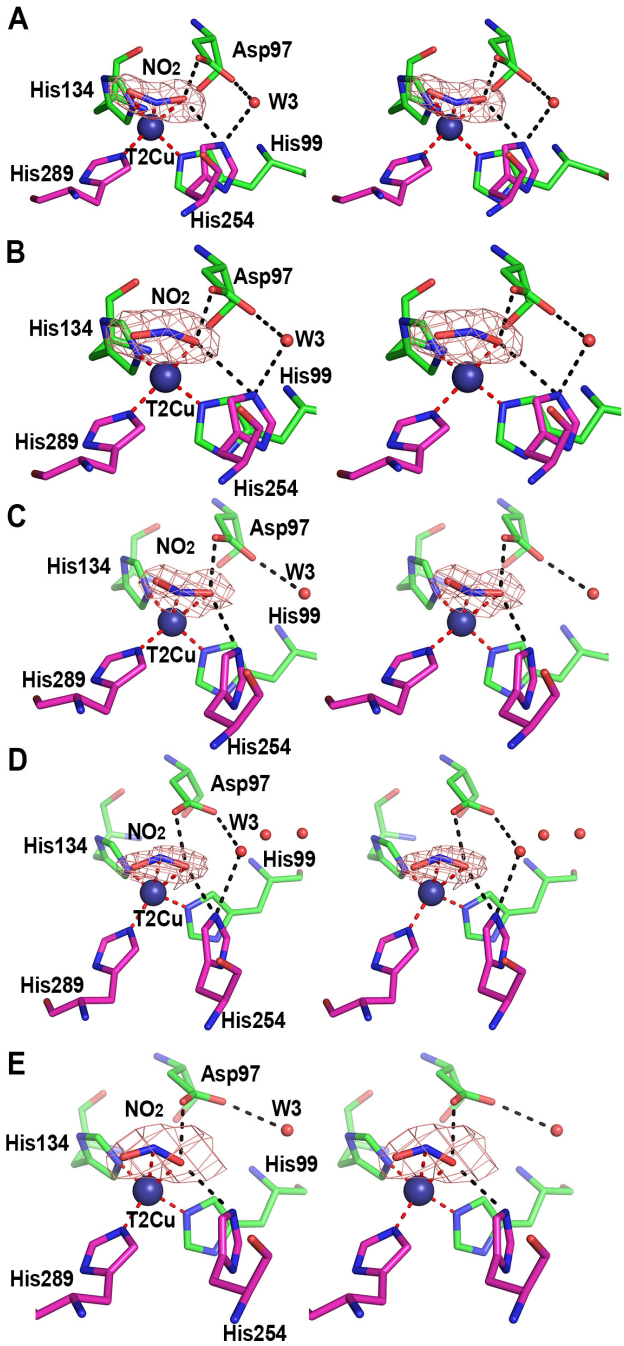

Figure S4. Details of nitrite binding in stereo view. A) *Rp*NiR-core molecules B and C showing nitrite bound in a "top-hat" configuration. **B)** *Rp*NiR-core molecules D and F showing nitrite bound in a "side-on" configuration. **C)** The full-length *Rp*NiR Y323A variant showing nitrite bound in "reverse-hat" configuration. **D)** The full-length *Rp*NiR Y323E variant showing nitrite bound in a "side-on" configuration. **E)** The full-length *Rp*NiR Y323F variant showing nitrite bound in a "side-on" configuration. An omit Fo-Fc electron density map is contoured at 5σ level around nitrite molecules. Residues from different CuNiR momomeric units are colored according to chains. T2Cu centres are shown as deep blue spheres, coordination bonds are shown as red dashed lines and hydrogen bonds as black dashed lines.

Active Site of the 'As-Isolated' Y323F Full-Length *Ralstonia Pickettii* Copper Containing Nitrite Reductase Variant.

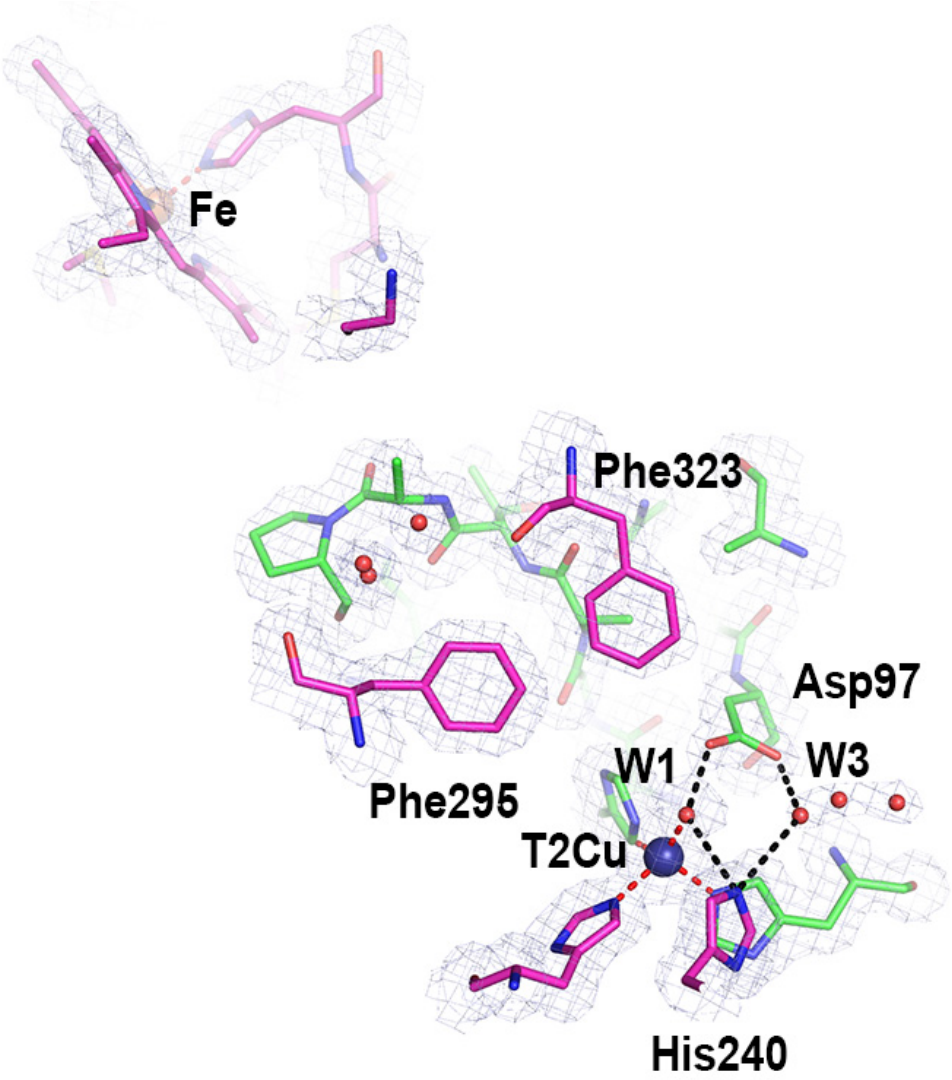

Figure S5. T2Cu site of 'as isolated' Y323F full-length *Rp*NiR variant. Hydrogen bonds are shown as black dotted lines, coordination bonds are in red, copper ions are shown as blue spheres and water molecules are small red spheres. A 2Fo-Fc electron density map is contoured at 1.0 σ level for the T2Cu site and haem region, and shown as light-grey mesh. Water W3 has three positions with partial occupancies.

Determination of Reduction Potentials of Copper and Haem Centres in *Ralstonia Pickettii* and *Achromobacter xylosoxidans* Copper Containing Nitrite Reductase and Cytochrome *c* Proteins

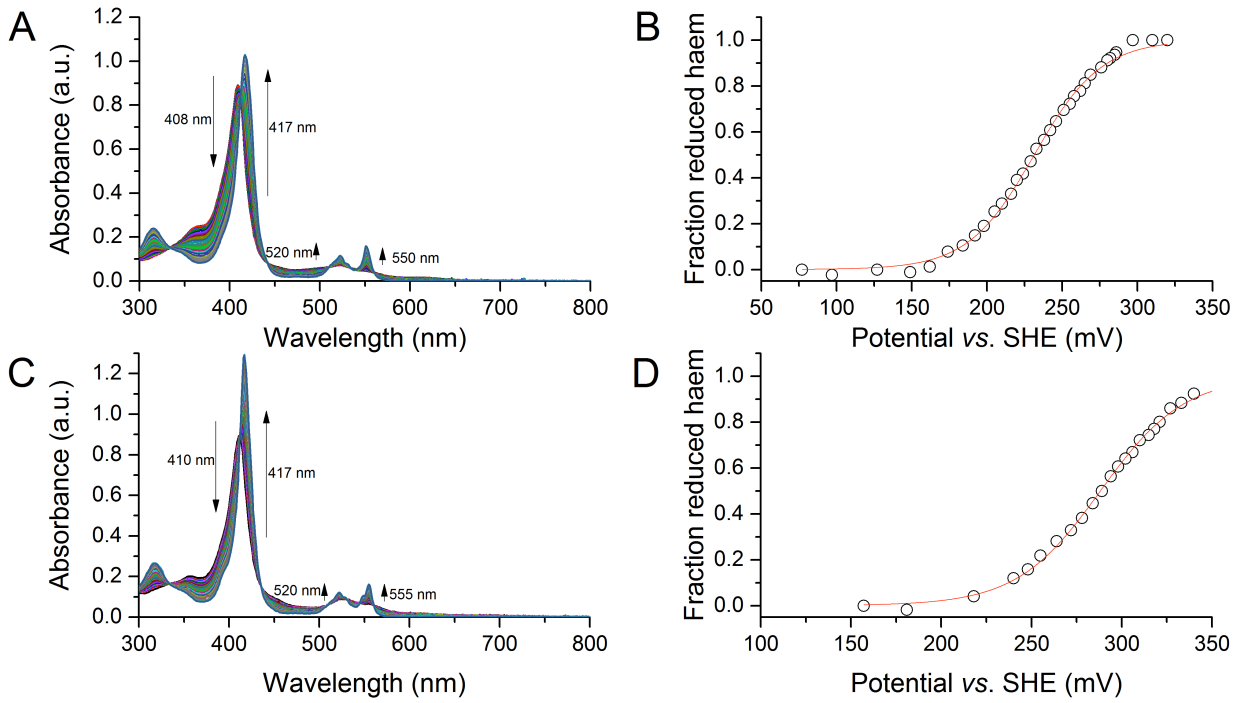

Figure S6. Determination of haem redox potential in *Alcaligenes xylosoxidans* cytochrome c_{551} and the constituent *Ralstonia pickettii* CuNiR cyt *c* protein. A) UV-Vis spectra changes of *Ax*cyt c_{551} during reduction with sodium dithionite. **B)** Fraction of the *Ax*cyt c_{551} Haem reduction as a function of potential. **C)** UV-Vis spectra changes of *Rp*NiR cyt *c* during reduction with sodium dithionite. **D)** Fraction of the *Rp*NiR *cyt c* haem reduction as a function of potential. The data in B (black circles) are fit to the Nernst equation (Eq. 4 in main manuscript; red line). Measurements were performed in 50 mM potassium phosphate buffer (pH 7.0), at 25 °C, with 7.5 µM *Ax*cyt c_{551}/*Rp*NiR cyt *c*. The *n* values determined from the Nernst equation are 1.0±0.1 and 1.1±0.1 for the haem cofactors present in *Ax*cyt c_{551} and in *Rp*NiR cyt *c* proteins, respectively.

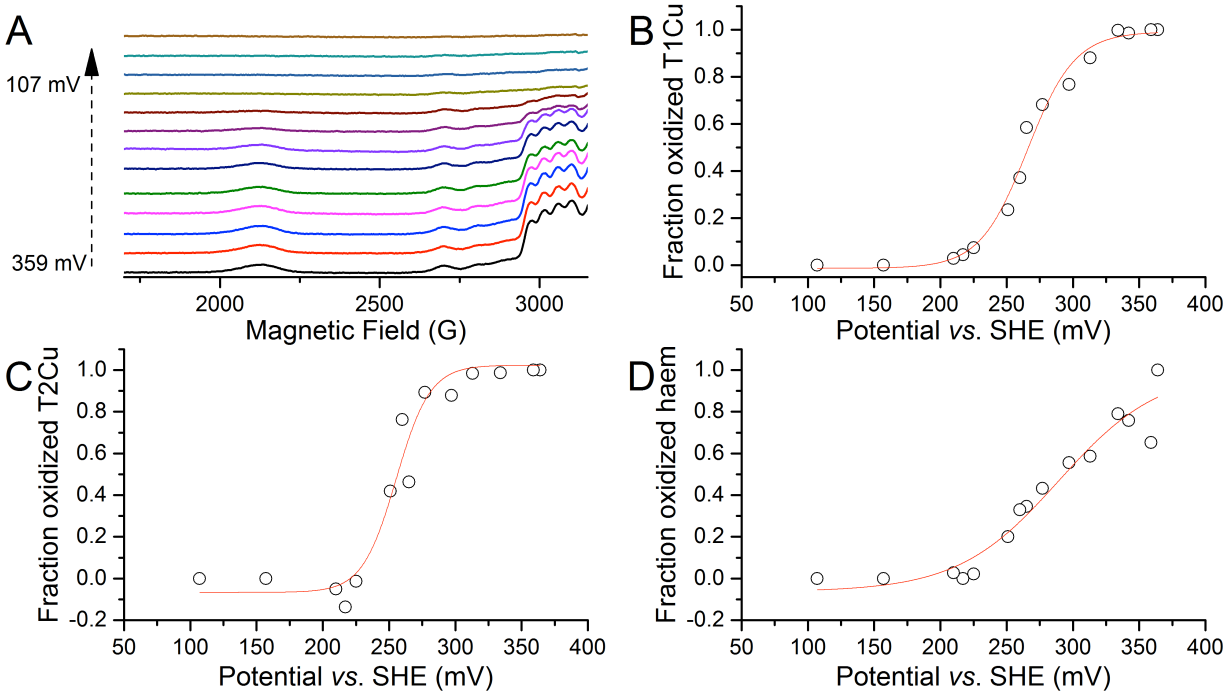

Figure S7. Determination of T1Cu, T2Cu and haem redox potential in *Ralstonia pickettii* CuNiR. A) EPR spectral changes of the *Rp*NiR T1Cu, T2Cu and the haem during reduction with sodium dithionite. **B)** Fraction of the *Rp*NiR T1Cu reduction as a function of potential. **C)** Fraction of the *Rp*NiR T2Cu reduction as a function of potential. **D)** Fraction of the *Rp*NiR haem reduction as a function of potential. The data in B, C and D (black circles) are fit to the Nernst equation (Eq. 4 in main manuscript; red line). All measurements were performed with *ca* 100 µM protein samples in 50 mM potassium phosphate buffer (pH 7.0), at 25 °C, which were frozen in liquid N_2 prior to EPR analysis. EPR spectra were recorded at 20 K on a Bruker EMX X-band EPR spectrometer. The microwave power was 0.5 mW, the modulation frequency 100 kHz, and the modulation amplitude 5 G. The *n* values determined from the Nernst equation are 0.7±0.2, 1.5±0.2 and 1.4±0.2 for the haem, T1 and T2Cu centres present in the full-length *Rp*NiR protein, respectively.

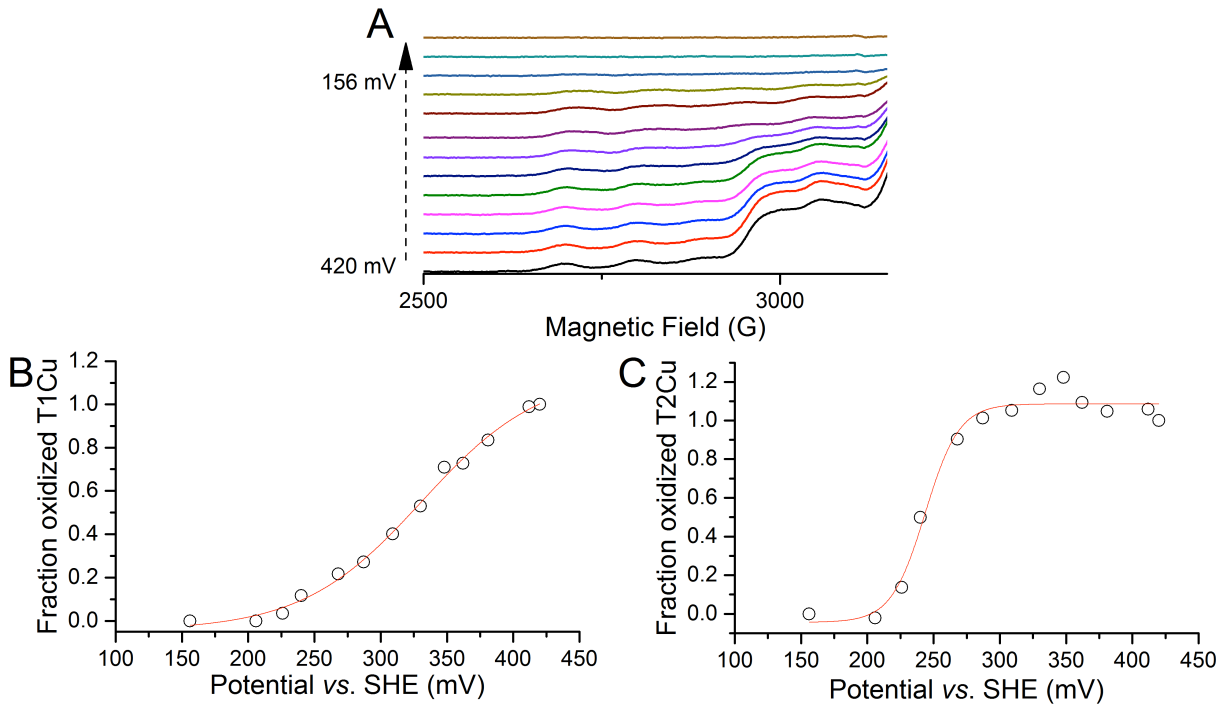

Figure S8. Determination of T1Cu and T2Cu redox potential in *Ralstonia pickettii* CuNiR-core. A) EPR spectral changes of the *Rp*NiR core1 T1Cu and T2Cu during reduction with sodium dithionite. **B)** Fraction of the *Rp*NiR T1Cu reduction as a function of potential. **C)** Fraction of the *Rp*NiR T2Cu reduction as a function of potential. The data in B and C (black circles) are fit to the Nernst equation (Eq. 4 in main manuscript; red line). All measurements were performed with *ca* 100 µM protein samples in 50 mM potassium phosphate buffer (pH 7.0), at 25 °C, which were frozen in liquid N_2 prior to EPR analysis. EPR spectra were recorded at 20 K on a Bruker EMX X-band EPR spectrometer. The microwave power was 0.5 mW, the modulation frequency 100 kHz, and the modulation amplitude 5 G. The *n* values determined from the Nernst equation are 0.6±0.2 and 1.2±0.1 for the T1 and T2Cu centres present in the *Rp*NiR-core protein, respectively.

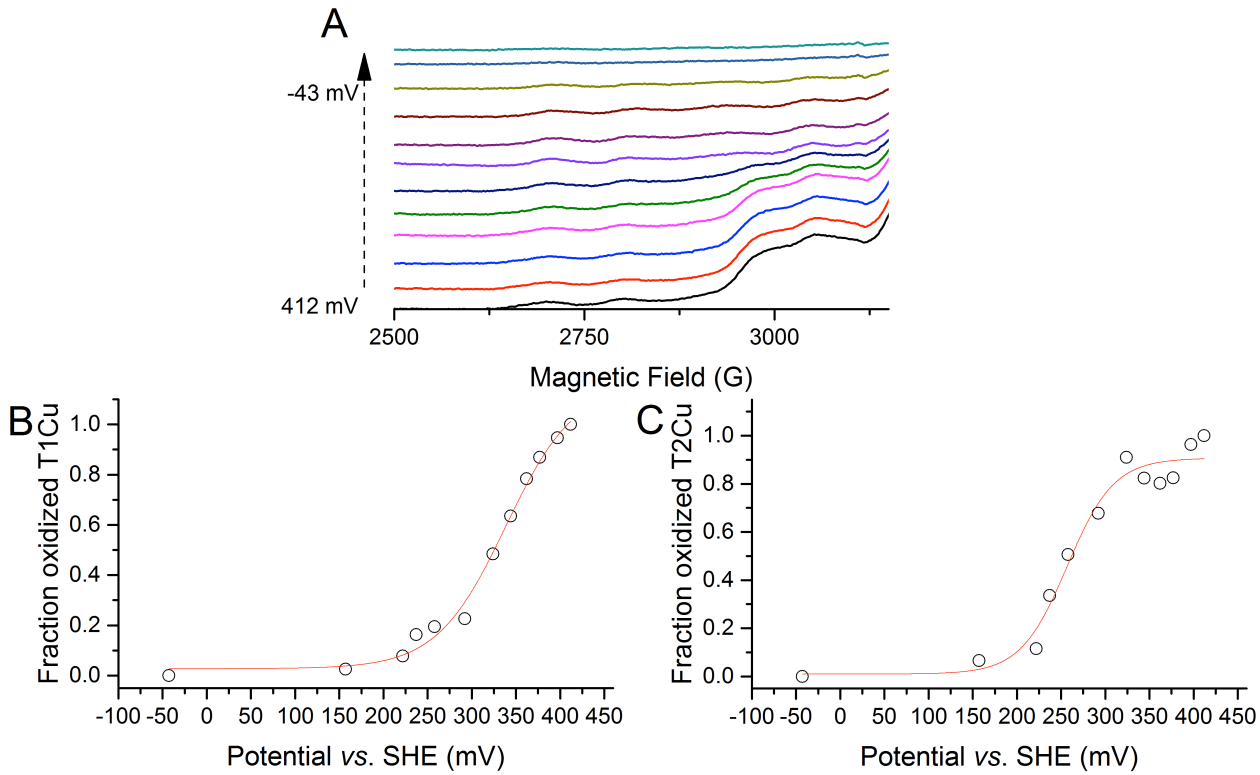

Figure S9. Determination of T1Cu and T2Cu redox potential in Y323F ***Ralstonia pickettii*** **CuNiR-core variant. A)** EPR spectral changes of the Y323F *Rp*NiR-core T1Cu and T2Cu during reduction with sodium dithionite. **B)** Fraction of the *Rp*NiR T1Cu reduction as a function of potential. **C)** Fraction of the *Rp*NiR T2Cu reduction as a function of potential. The data in B and C (black circles) are fit to the Nernst equation (Eq. 4 in main manuscript; red line). All measurements were performed with *ca* 100 µM protein samples in 50 mM potassium phosphate buffer (pH 7.0), at 25 ºC, which were frozen in liquid N_2 prior to EPR analysis. EPR spectra were recorded at 20 K on a Bruker EMX X-band EPR spectrometer. The microwave power was 0.5 mW, the modulation frequency 100 kHz, and the modulation amplitude 5 G. The *n* values determined from the Nernst equation are 0.7±0.2 and 1.0±0.3 for the T1 and T2Cu centres present in the Y323F *Rp*NiR-core protein, respectively.

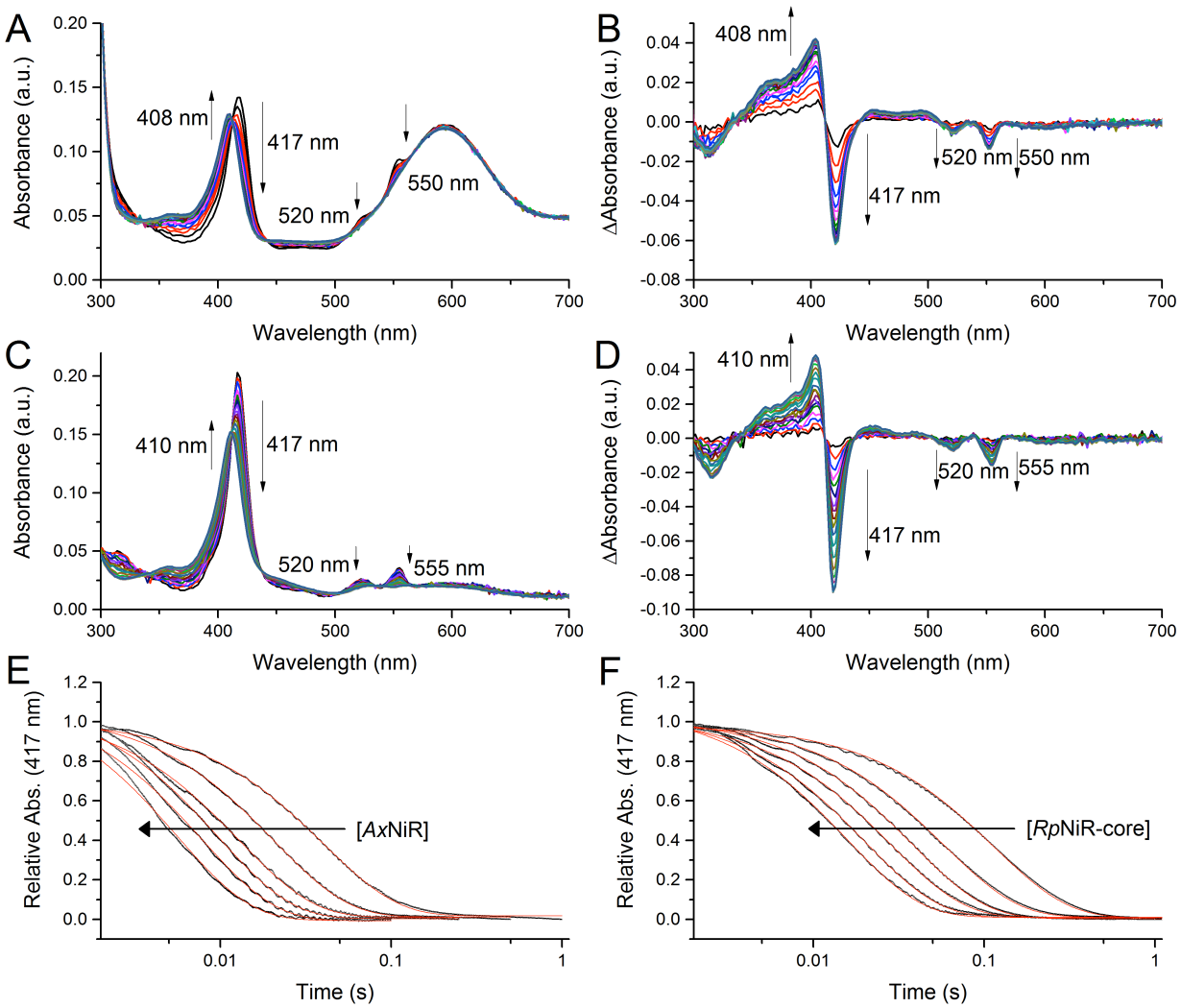

Figure S10. Photodiode array (PDA) spectra and example stopped-flow transients for the reaction between reduced *Ax*cyt c_{551} and oxidised *Ax*NiR. A) Raw PDA spectra showing UV-Vis changes for the reaction between reduced *Ax*cyt c_{551} and oxidised *Ax*NiR. **B)** Absorbance difference spectra, relative to the spectrum at 5 ms, derived from data in A. **C)** Raw PDA spectra showing UV-Vis changes for the reaction between reduced *Ax*cyt c_{551} and oxidised *Ax*NiR. **D)** Absorbance difference spectra, relative to the spectrum at 5 ms, derived from data in C. **E)** Example stopped-flow transients and corresponding single exponential fits for the reaction between *Ax*NiR and *Ax*cyt c_{551}. **F)** Example stopped-flow transients and corresponding single exponential fits for the reaction between the *Rp*NiR-core and the *Rp*NiR cyt *c* protein. Conditions: 1 µM *Ax*cyt c_{551} (final concentration) mixed with 10-80 µM oxidised *Ax*NiR (final concentration) in 50 mM potassium phosphate buffer (pH 7.0), 50 mM potassium chloride, at 10 °C. For PDA experiments, 20 µM oxidised NiR protein was used and data was recorded over a 1 s timeframe.

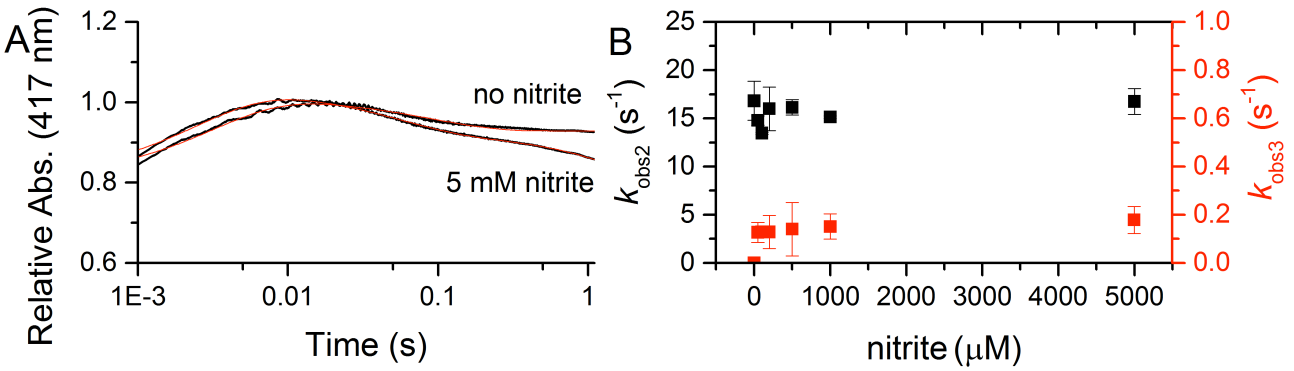

Figure S11. Laser flash photolysis method to monitor Haem to T1Cu electron transfer in *Ralstonia pickettii* copper containing nitrite reductase. A) Example transients (black) and the corresponding exponential fits (red) for the laser flash photolysis assay used to monitor haem to T1Cu electron transfer. With no nitrite present, only one kinetic phase is observed in the haem to T1Cu electron transfer reaction (shown by a single exponential for the decrease in absorbance at 417 nm in absence of nitrite in A.). Conversely, when nitrite is present, there is an additional kinetic phase observed with a slow rate constant (shown as a double exponential for the decrease in absorbance at 417 nm in presence of nitrite in A.) that is similar to the steady state rate of turnover per *Rp*NiR trimer (see Figure 5). **B)** Nitrite dependence on the rate of haem to T1Cu electron transfer in *Rp*NiR. Measurements were performed on 17 μM of *Rp*NiR in 50 mM potassium phosphate buffer (pH 7.0), with [KCl]+[KNO_2] = 50 mM, at 10 °C. Reactions were initiated by un-caging of NADH in the dark with a laser flash photolysis excitation at 335 nm^2 and were tracked by following changes in the cytochrome *c* haem soret peak at 417 nm.

SAXS Data from the Full-Length *Rp*NiR in Solution

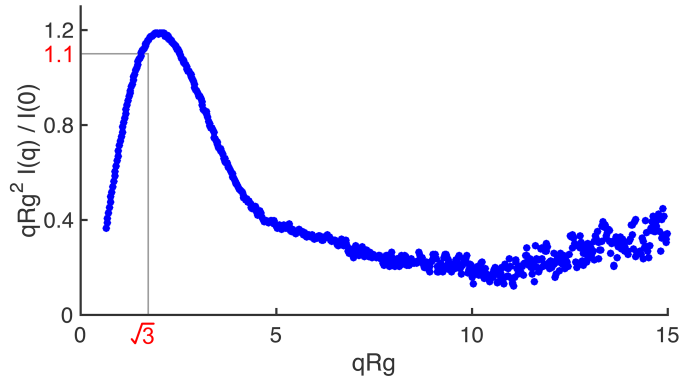

Figure S12. Dimensionless Kratky plot of SAXS from full-length *Rp*NiR in solution. A compact protein has a maximum at √3 and 1.1. Movement of the peak into the positive quadrant of the graph is indicative of unfolding or conformational flexibility. Data taken from [3].

Inter Copper Electron Transfer In The *Ralstonia Pickettii* Copper Containing Nitrite Reductase Core Proteins

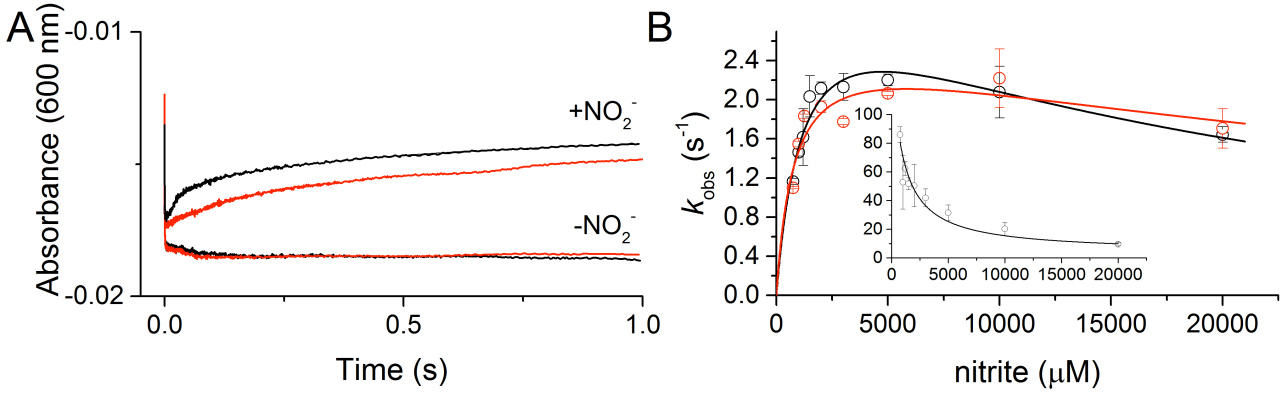

Figure S13. Inter-copper electron transfer in the *Ralstonia pickettii* copper nitrite reductase core proteins. A) Example transients and corresponding exponential fits for the T1Cu to T2Cu electron transfer reaction in the *Rp*NiR-core (black) and Y323F *Rp*NiR-core (red) constructs. **B)** Substrate dependence of T1 to T2Cu electron transfer rate in the *Rp*NiR-core (black) and Y323F *Rp*NiR-core constructs. The insert in B) shows the faster rate constants associated with inter-copper electron transfer in the *Rp*NiR-core construct.

Nitrite Affinity in the 1-Electron Reduced State of *Ralstonia Pickettii* Copper Containing Nitrite Reductase

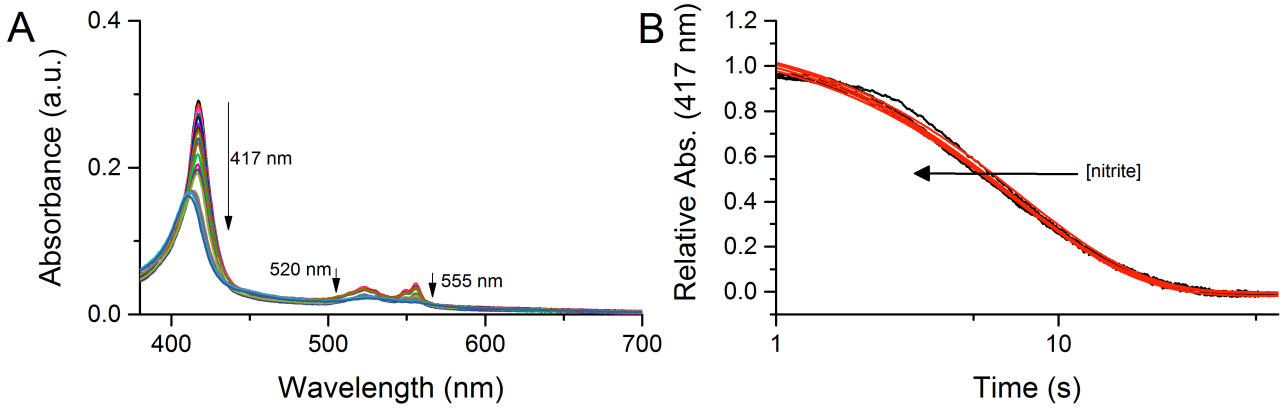

Figure S14. A) UV-Vis spectral changes associated with titration of 1-electron reduced *Rp*NiR with nitrite. B) Example stopped-flow transients for the reaction between 1-electron reduced *Rp*NiR and nitrite. Measurements were performed in 50 mM potassium phosphate buffer (pH 7.0), at 10 °C, with 0.5 μM (or 2 μM for spectral titration presented in A) of 1-electron reduced *Rp*NiR and various nitrite concentrations.

Kinetic Model Suggesting Third Site Reactivity in *Ralstonia Pickettii* Copper Containing Nitrite Reductase

Stopped-flow was used to explore the kinetics of electron transfer between the haem and the T1Cu. The stopped-flow limiting rate constant (k_{lim} 0.34 ± 0.02 s^{-1}) for haem re-oxidation is one-third the value of the steady-state turnover value (k_{cat} 1.1 ± 0.03 s^{-1}). This suggests only one of the three active sites in the trimer is competent in electron transfer from haem to T2Cu at any time i.e. 'one-third active site reactivity'. This one-third site reactivity might be more widely operative in CuNiR proteins as similar observations have been made in single molecule electrochemical studies of NiR activity but was considered to arise from heterogeneity of binding to the electrode.[4] Also, in the X-ray crystallographic structure of the *Ax*NiR–cyt c_{551} complex only one cytochrome *c* protein is found associated with the core CuNiR protein (Figure 1A).[5] It has been argued that this is attributed to crystal packing. Our findings with *Rp*NiR might also suggest a role for fractional reactivity in the observed stoichiometry of the *Ax*NiR–cyt c_{551} complex. See below for kinetic model:

The reaction can be modelled as a sequential 3-step irreversible reaction:

$$\mathrm{A} + \mathrm{SD} \overset{k_1}{\rightarrow} \mathrm{B} + \mathrm{SD} \overset{k_2}{\rightarrow} \mathrm{C} + \mathrm{SD} \overset{k_3}{\rightarrow} \mathrm{D} \overset{fast}{\longrightarrow} \mathrm{A} \qquad \text{(Eq. S1)}$$

Where A, B, C and D are the fully reduced ($Fe(II)_3$), $Fe(II)_2$/Fe(III), Fe(II)/$Fe(III)_2$, and fully oxidized species, respectively and SD is sodium dithionite.

The rate of sodium dithionite consumption is then described by:

$$\frac{d}{dt}[\mathrm{SD}] = -k_1[\mathrm{A}][\mathrm{SD}] - k_2[\mathrm{B}][\mathrm{SD}] - k_3[\mathrm{C}][\mathrm{SD}] \qquad \text{(Eq. S2)}$$

This directly describes the reaction velocity described under steady-state conditions. However, in the steady state assay, V_{max} is independent of [SD], so each step in Eq. S1 is effectively first order. Consequently:

$$\frac{d}{dt}[\mathrm{SD}] = -k_1{}'\,[\mathrm{A}] - k_2{}'\,[\mathrm{B}] - k_3{}'\,[\mathrm{C}] \qquad \text{(Eq. S3)}$$

As the concentration of each monomer in the trimer is the same, [A] = [B] = [C] = [monomer]:

$$\frac{d}{dt}[\mathrm{SD}] = -(k_1{}' + k_2{}' + k_3{}')[\mathrm{monomer}] \qquad \text{(Eq. S4)}$$

Finally, if the active sites are equivalent, then $k_1{}'$ = $k_2{}'$ = $k_3{}'$ and:

$$\frac{d}{dt}[\mathrm{SD}] = -3k_1{}'\,[\mathrm{monomer}] \qquad \text{(Eq. S5)}$$

If the stopped-flow experiments report on k_1', then the observed rate constants will be 1/3 that observed under steady state turnover conditions.

References

(1) Robert, X.; Gouet, P. Deciphering Key Features in Protein Structures with the New ENDscript Server. *Nucleic Acids Res.* **2014**, *42*, W320–W324.

(2) Leferink, N. G. H.; Han, C.; Antonyuk, S. V.; Heyes, D. J.; Rigby, S. E. J.; Hough, M. A.; Eady, R. R.; Scrutton, N. S.; Hasnain, S. S. Proton-Coupled Electron Transfer in the Catalytic Cycle of *Alcaligenes Xylosoxidans* Copper-Dependent Nitrite Reductase. *Biochemistry* **2011**, *50*, 4121–4131.

(3) Han, C.; Wright, G. S. A.; Fisher, K.; Rigby, S. E. J.; Eady, R. R.; Samar Hasnain, S. Characterization of a Novel Copper-Haem c Dissimilatory Nitrite Reductase from *Ralstonia Pickettii*. *Biochem. J* **2012**, *444*, 219–226.

(4) Krzemiński, Ł.; Ndamba, L.; Canters, G. W.; Aartsma, T. J.; Evans, S. D.; Jeuken, L. J. C. Spectroelectrochemical Investigation of Intramolecular and Interfacial Electron-Transfer Rates Reveals Differences between Nitrite Reductase at Rest and during Turnover. *J. Am. Chem. Soc.* **2011**, *133*, 15085–15093.

(5) Nojiri, M.; Koteishi, H.; Nakagami, T.; Kobayashi, K.; Inoue, T.; Yamaguchi, K.; Suzuki, S. Structural Basis of Inter-Protein Electron Transfer for Nitrite Reduction in Denitrification. *Nature* **2009**, *462*, 117–120.